research papers

Multiple-electron excitation in X-ray absorption: a screened model of the core-hole–photoelectron potential

Mervyn Roy* and S. J. Gurman

Department of Physics and Astronomy, University of Leicester, University Road, Leicester, England. E-mail: mr6@le.ac.uk

The probability of secondary electron shake-off in X-ray absorption is calculated using a model form for the time- and energy-dependent core-hole–photoelectron potential, screened by the single plasmon pole dielectric function of the surrounding material. The resultant excitation probabilities are related to the energy-dependent intrinsic loss function in EXAFS data analysis and compared with experiment. Reasonable agreement is obtained close to the absorption edge although the calculation is less accurate at higher photon energies. The theory described allows the losses to be calculated with little computational effort, making the method suitable for routine EXAFS data analysis.

1. Introduction

X-ray absorption theory is usually given in purely one-electron terms. This gives very good results for the X-ray absorption coefficient (Gurman, 1983) and reasonable results for the extended X-ray absorption fine structure (EXAFS) *except* for the amplitude. In a single-electron formalism, Coulomb interactions between the created photoelectron and the bystander electrons are neglected. These interactions can give rise to multiple electron excitations which remove photoelectrons from the elastic-scattering channel, hence reducing the primary-channel EXAFS (Rehr *et al.*, 1978). In EXAFS data analysis, excitations at the absorbing atom (intrinsic losses) are usually accounted for by multiplying the single-electron result by a constant loss factor, s_o^2, while the losses at the scattering atoms (extrinsic losses) are included by introducing an imaginary part to the scattering potential. A constant value for the intrinsic loss factor is, however, a poor approximation, especially close to the X-ray absorption edge. In this paper we investigate the energy dependence of s_o^2.

In a previous paper (Roy *et al.*, 2001) we extended the time-dependent perturbation theory of Thomas (1984) to describe the energy dependence of the intrinsic losses for all atoms using a simple generic model. In this formalism, however, the strength of the core-hole–photoelectron potential was not given explicitly, but had to be included by normalizing the results to experiment or theory (Roy & Gurman, 1997) in the high-energy limit. In the present paper we attempt to rectify this problem by using a model form for this potential, screened by the energy- and frequency-dependent dielectric function. We know that the previous form of the theory gives a good description of the EXAFS losses. In this paper we attempt to obtain an equally good description without the inclusion of any 'fiddle factors'. The aim is to describe the inherently difficult problem of multiple electron excitations in terms of a physically intuitive theory, following such authors as Gadzuk & Sunjic (1972), Noguera & Spanjaard (1981) and Vatai (1988). The form of the theory described is simple enough to be easily programmable and can be evaluated

sufficiently quickly to be of use in routine data analysis. It is found to give reasonable agreement with experiment for rare-gas atoms.

In the present paper (as in the previous work) we calculate only shake-off transition probabilities. The shake-up, or bound-to-bound, transitions are much less probable than excitations into the continuum (Carlson *et al.*, 1968; Hasnain, 1990) and are usually ignored for EXAFS data-analysis purposes (Hayes & Boyce, 1982). Also, shake-up transitions typically involve only the weakly bound initial states. The energies of these bound-to-bound transitions will therefore tend to be small, and the photoelectron energy will not differ from that of the elastically scattered primary photoelectron by more than a few eV. Thus, experimentally, the two contributions to the EXAFS signal tend not to be resolved and, in practice, the shake-up channels cause no diminution to the measured EXAFS signal.

The calculation of the EXAFS intrinsic loss factor is identical to that of the probability of multiple-electron excitation, a problem which has been studied by many authors. Most of these calculations, however, are complicated and computationally intensive (*e.g.* Chang & Poe, 1975; Carter & Kelly, 1977) and are therefore unsuited for EXAFS data-analysis purposes. Recently, work has been done on a full description of EXAFS losses including the intrinsic and extrinsic losses and the interference (Hedin, 1989) between these terms (*e.g.* Fujikawa *et al.*, 2000; Natoli, 1995; Newville *et al.*, 1993; Tyson *et al.*, 1992); however, again we are unaware of any of these methods currently being used for routine EXAFS data analysis. At present most EXAFS data-analysis programs use the Hedin–Lundqvist exchange and correlation potential to model inelastic effects. Empirically, this potential includes all the losses to the EXAFS amplitude (Roy & Gurman, 2001) although it was designed to model only the extrinsic losses. The absolute accuracy of the Hedin–Lundqvist potential is therefore uncertain (Tyson, 1991).

2. Theory

In the standard EXAFS problem a photon of frequency ω is absorbed by an atom. The photon excites an electron from a given initial state, φ_i, into a continuum state of energy $\omega - |\omega_i|$. Following the photo-ionization, the resulting core-hole–photoelectron system acts as a perturbation on the other, passive, electrons in the absorbing atom. We approximate this time-dependent perturbation with a screened model potential and use first-order time-dependent perturbation theory to calculate the probability of exciting each of the secondary electrons.

The temporal variation of the potential arises because the photoelectron takes a finite time to leave the atom, the time depending on the size of the atom and the speed of the photoelectron. In the same way as in the previous paper (Roy *et al.*, 2001), following Gadzuk & Sunjic (1975) or Thomas (1984), we approximate the *unscreened* time- and position-dependent perturbation $V(r, t)$ as a product of time-dependent and position-dependent parts,

$$V(r, t) = V(r)f(t), \tag{1}$$

where we assume

$$f(t) = [1 - \exp(-t/t_o)]\Theta(t). \tag{2}$$

With this form of the potential the passive electrons see the full core-hole potential, $V(r)$, as $t \to \infty$ when the photoelectron has left the atom. In equation (2) the characteristic time, $t_o = R_c/v$, where R_c is a characteristic distance of the atom and represents the size of the orbital of passive electrons. v is the speed of the photoelectron, which, following Thomas (1984), we have assumed to be time independent.

Finally, $\Theta(t)$ is the Heaviside step function which ensures that the perturbation is switched on at $t = 0$ when the photoelectron is created.

Thomas (1984) treats R_c as an adjustable parameter. We, however, take R_c to be the mean radius of each atomic orbital, arguing that the majority of the interaction between the passive electron and the photoelectron will take place within this radius. We set R_c from the binding energy of each orbital, using the relation for hydrogenic wavefunctions, $R_c = n_o/(2E_o)^{1/2}$, where E_o is the binding energy and n_o is the principle quantum number of each orbital.

The unscreened core hole can be described by a simple coulomb $1/r$ potential. However, using this potential for the core hole gives values for the probabilities which are much too large. The $1/r$ perturbation is too strong: the majority of passive electrons will not see a bare core hole because of the screening effects of the other passive electrons. This screening will, in general, be energy dependent. We can model the screening using the single plasmon pole dielectric function of Hedin & Lundqvist (1969). This energy-dependent dielectric function will reduce the magnitude of the hole potential seen by the passive electrons. It will also introduce some many-body effects into our single-electron theory.

To screen the time-dependent potential we must first write it in Fourier transform,

$$V(q, \omega) = \frac{4\pi}{iq^2}\left(\frac{1}{\omega} - \frac{1}{\omega - it_o^{-1}}\right). \tag{3}$$

The screened time-dependent perturbation is then given by

$$V(r, t) = \frac{1}{(2\pi)^4}\int d\mathbf{q}\,d\omega\,\exp(i\mathbf{q}\cdot\mathbf{r})\exp(i\omega t)V(q,\omega)\varepsilon^{-1}(q,\omega), \tag{4}$$

where $\varepsilon^{-1}(q, \omega)$ is the causal single plasmon pole dielectric function,

$$\varepsilon^{-1}(q, \omega) = 1 + \frac{\omega_p^2}{2(\omega - i\eta)}\left(\frac{1}{\omega - \omega_q - i\eta} + \frac{1}{\omega + \omega_q - i\eta}\right), \tag{5}$$

ω_p is the appropriate plasma frequency and ω_q is the q-dependent plasmon excitation energy.

Using the above results we can calculate the probability of a multiple-electron excitation following the creation of the core-hole–photoelectron system. As discussed in the previous work (Roy *et al.*, 2001), time-dependent perturbation theory gives the probability amplitude of a passive electron being excited from an atomic orbital, $|\varphi_o\rangle$, into an excited state, $|\psi_n\rangle$, as

$$a_{no} = \int_o^\infty \exp[i(\omega_{no} + i\eta')t]\langle\psi_n|V(r,t)|\varphi_o\rangle\,dt, \tag{6}$$

where the convergence factor $\exp(-\eta' t)$ corresponds physically to the finite core-hole lifetime. Substituting result (4) for $V(r, t)$ and integrating over time we obtain the probability amplitude as

$$a_{no} = \left\langle\psi_n\left|\int\frac{d\mathbf{q}\exp(i\mathbf{q}\cdot\mathbf{r})}{\omega_{no}(2\pi)^4}\int d\omega\frac{\omega V(q,\omega)\varepsilon^{-1}(q,\omega)}{\omega_{no} + \omega + i\eta'}\right|\varphi_o\right\rangle. \tag{7}$$

The ω integral above may be performed using contour integration by closing contours in the lower half plane. All the poles in $V(q, \omega)$ and $\varepsilon^{-1}(q, \omega)$ must lie in the upper half plane so that $V(r, t)$ is zero for $t < 0$. We therefore simply pick up a contribution from the pole at $\omega = -\omega_{no} - i\eta'$ to obtain

$$a_n = \frac{i}{(2\pi^3)}\left\langle\psi_n\left|\int d\mathbf{q}\exp(i\mathbf{q}\cdot\mathbf{r})V(q,-\omega_{no})\varepsilon^{-1}(q,-\omega_{no})\right|\varphi_{l_o}\right\rangle. \tag{8}$$

We define a slightly simpler form for ω_q to that normally used (Hedin & Lundqvist, 1969) so that we may evaluate the q-integrals analytically. We choose

$$\omega_q^2 = \omega_p^2 + q^4/4, \tag{9}$$

which exhibits the correct high and low q limits and should therefore give a good approximation to the true excitation frequencies. As we are dealing with atoms and not a free-electron gas we make use of the local density approximation to write the plasma frequency ω_p in terms of the radially varying atomic charge density.

Then, using this approximate form for ω_q and taking the infinitesimals in $\varepsilon^{-1}(q, \omega)$ to zero we can integrate equation (8) directly using a result from Gradsteyn & Ryzhik (1965),

$$a_n = \frac{it_o^{-1}}{\omega_{no}(\omega_{no} + it_o^{-1})}\left\langle\psi_n\left|\frac{\omega_{no}^2 - \omega_p^2(r)f(r,\omega_{no})}{r[\omega_{no}^2 - \omega_p^2(r)]}\right|\varphi_o\right\rangle, \tag{10}$$

where

$$f(r,\omega_{no}) = \tfrac{1}{2}\exp(-br) + \tfrac{1}{2}\cos(br) \qquad \omega_{no} > \omega_p(r)$$
$$= \exp(-br/2^{1/2})\cos(br/2^{1/2}) \qquad \omega_{no} < \omega_p(r), \tag{11}$$

and

$$b^4 = |\omega_{no}^2 - \omega_p^2|. \tag{12}$$

There are weak divergences in the r-integrand for both $\omega_{no} > \omega_p$ and $\omega_{no} < \omega_p$ of the form $|\omega_{no}^2 - \omega_p^2(r)|^{1/4}$. However, the integrals are easily evaluated numerically using a standard Romberg integration routine (Press *et al.*, 1992).

At this point we concentrate on the secondary electron shake-off and ignore the possibility of bound-to-bound transitions. We can then calculate the probability of exciting any of the secondary electrons into any continuum state following the absorption of a photon in the same way as in Roy *et al.* (2001). We find

$$P_T(\omega) = \frac{1}{2\pi}\sum_i\frac{\mu_o^i(\omega)}{\mu_o(\omega)}\sum_{n_o,l_o}n_{(n_o,l_o)}\int_o^{kmax}\frac{k^2t_o^{-2}}{\omega_{ko}^2(\omega_{ko}^2 + t_o^{-2})}$$
$$\times\left|\int R_{l_o}(k,r)\varphi_{l_o}(r)\left[\frac{\omega_{ko}^2 - \omega_p^2(r)f(r,k)}{r[\omega_{ko}^2 - \omega_p^2(r)]}\right]r\,dr\right|^2 dk, \tag{13}$$

where the angular parts of the spatial integral have been evaluated to give $\delta_{l_n l_o}$. φ_{l_o} is a bound atomic orbital while $R_{l_o}(k, r)$ is the photoelectron final state. In numerical work we take the initial states from tables by Clementi & Roetti (1974) while the photoelectron final state may be easily calculated from the Schrödinger equation in the Hartree approximation using a standard Runge–Kutta routine.

A photon incident on an atom may excite electrons from any occupied core state, φ_i, provided that $\omega > |\omega_i|$. To compare directly with experiment, we have therefore weighted the probability of exciting a secondary electron given that the photoelectron is from state φ_i with the probability that the photon is absorbed by the electron in state φ_i. Thus μ_o^i is the contribution to the total atomic absorption coefficient, μ_o, from all electrons in the initial state φ_i.

In EXAFS experiments, where the initial photoelectron state is known, the $\sum_i\mu_o^i/\mu_o$ term in the equation above may be removed to give $P(\omega)$, the contribution to the secondary excitation probability from a given edge. Only those photoelectrons which do not excite passive electrons into the continuum contribute to the EXAFS signal, thus the amplitude reduction factor is simply the probability that none of the secondary electrons are excited,
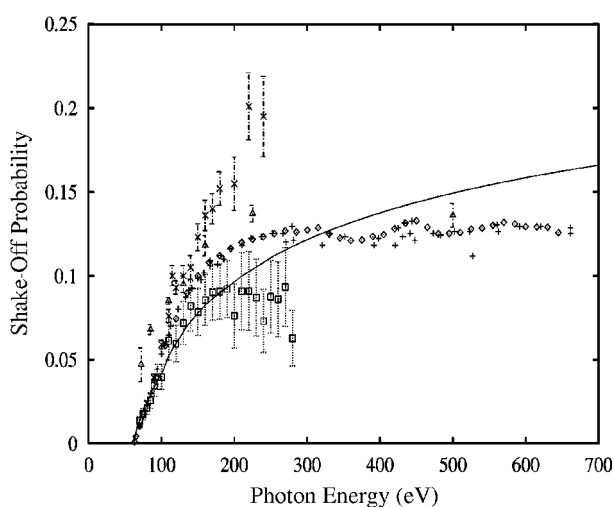
$$s_o^2(\omega) = 1 - P(\omega). \tag{14}$$

3. Results

In this section we calculate the secondary electron excitation probabilities using equation (13) and compare with experimental data for the neon L edge and argon K edge. We also examine the energy-dependent amplitude reduction factor and calculate an example EXAFS spectrum for copper. We choose these systems primarily because of the availability of experimental data, but also to demonstrate the flexibility of the method: the secondary excitation probabilities may be easily calculated for any absorption edge of any element.

3.1. Secondary electron excitation probabilities

Fig. 1 compares calculated and measured shake-off probabilities for neon following an L-edge photoionization. The magnitudes of the calculated results agree fairly well with the experimental data over the whole of the energy range investigated, certainly to the level of scatter in the various experimental results. The calculated result for the neon L edge matches the data well at low energies and appears to exhibit the correct energy dependence up to a photon energy of $\sim$300 eV. The theoretical result has not, however, reached its sudden limit even by 700 eV above threshold but gives shake-off probabilities which are still rising with energy. This could be due to a fault in our model dielectric function. With the simplified single plasmon pole, LDA, dielectric function [equation (5)] it is possible that we are under-screening the core hole at high primary photoelectron energies.

Fig. 2 shows the shake-off probabilities against photon energy following an argon K-edge photoionization. The experimental results (points with error bars) have been measured by Armen *et al.* (1985) while the dotted line is reproduced from Roy *et al.* (2001). The calculated result, using the screened core hole, gives a reasonable approximation to the measured data although the energy dependence is not as good as for the neon L edge. Again, the calculated excitation probabilities are still rising at high photoelectron energies where we might have expected them to have reached their sudden limit. Over the whole of the energy range investigated the screened core hole

result is not as good as the simple Thomas approximation result from the previous paper. However, the screened core hole result appears to better match the energy dependence of the experimental data at low energies, up to about 70 eV above the edge.
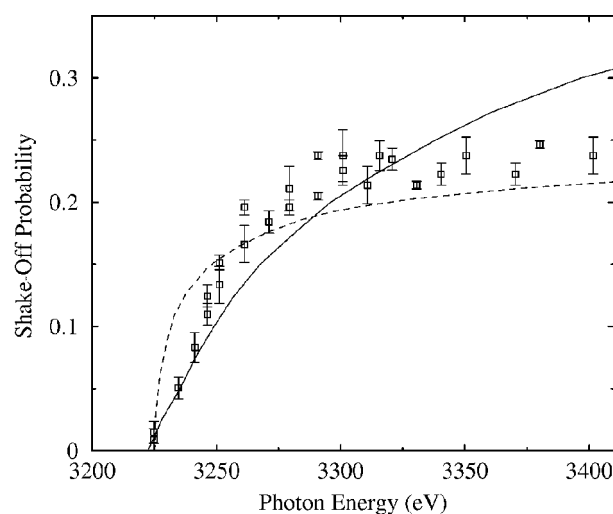
3.2. Amplitude reduction factor

From equation (14) we can calculate the energy-dependent amplitude reduction factor. To obtain the total loss factor for the EXAFS amplitude we must also account for extrinsic losses to the photoelectron beam at the scattering atom and in the medium in between the central and scattering atoms. We do this by multiplying by a mean-free-path term, $\exp[-2(r_1 - r_o)V_{PI}/k]$, where r_1 is the distance to the scattering atom, r_o is the muffin tin radius of the central atom and V_{PI} is the magnitude of a constant imaginary potential, usually taken to be 4 eV.

Once we have obtained the total loss factor we can compare EXAFS amplitudes using the screened core hole amplitude reduction factor with those found experimentally and those calculated using the standard Hedin & Lundqvist (1969) exchange and correlation potential used in most current EXAFS data-analysis programs [*e.g.* *EXCURV*98 (Binsted, 1998)]. This comparison is shown in Figs. 3 and 4 for copper.

The Daresbury program *EXCURV*98 was used to calculate an EXAFS spectrum for Cu foil with both the Hedin–Lundqvist (solid line) and the $X\alpha$ potentials. We used only the first shell of scattering atoms in order to obtain an unambiguous value for the distances used in the mean-free-path term. The refined fit gave a nearest-neighbour distance of $r_1 = 2.541 \pm 0.006$ Å, a first-shell coordination number of $n_1 = 11.3 \pm 1.5$, a Fermi energy of $E_f = -13.2 \pm 0.8$ eV and a Debye–Waller factor of $a_1 = 0.016 \pm 0.002$ Å^2. These parameters were then used as input to calculate the spectra using the real $X\alpha$ potential which includes no losses.

Fig. 3 shows a direct comparison between loss factors calculated using the screened core hole and those given by the Hedin–Lundqvist potential. To obtain the data points we have ratioed the peak heights of the EXAFS spectra calculated with the Hedin–Lundqvist potential to the equivalent peak heights of the spectra calculated with the $X\alpha$ potential. The solid line shows the result for the loss factor calculated
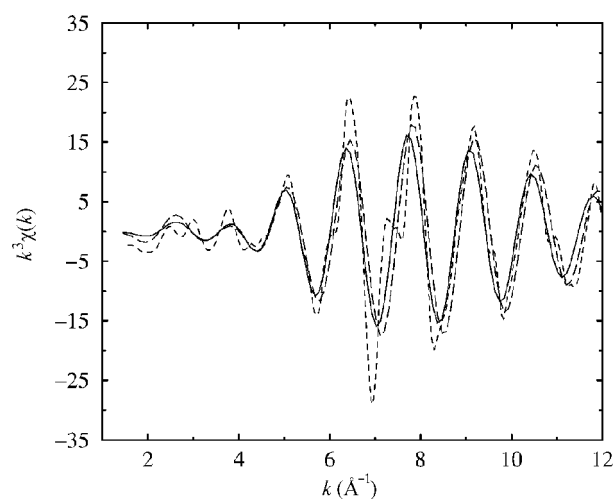

Figure 1
The probability of secondary electron excitation as a function of photon energy following the creation of a photoelectron from the L shell in neon. The solid line shows the result calculated using equation (13). The points are experimental data: diamonds from Bartlett *et al.* (1992), crosses from Samson *et al.* (1992), open squares with error bars from Holland *et al.* (1979), crosses with error bars from Wight & Van der Viel (1976) and triangles with error bars from Carlson *et al.* (1968).

Figure 2
The probability of secondary electron excitation as a function of photon energy for the argon K-edge. The points are experimental data from Armen *et al.* (1985). The solid line shows the result calculated using a screened core hole potential [equation (13)] while the dashed line is reproduced from Roy *et al.* (2001).

using the screened core hole and multiplied by the appropriate mean-free-path term to describe the losses outside of the central muffin tin.

Within the range of an EXAFS spectra the model energy-dependence calculation gives reasonable agreement with the losses obtained using the Hedin–Lundqvist potential, at least to the $\pm10\%$ level required by EXAFS calculations. The energy dependence of the total calculated loss factor is unphysical at small k because of the constant value for V_{PI} used in the mean-free-path term. This completely kills the EXAFS as $k \to 0$. To model the mean-free-path term more accurately we need an energy-dependent V_{PI}, the simplest form being one which simply cuts off at the binding energy of the most weakly bound state. Below this energy, no inelastic scattering is possible and thus we obtain no losses to the EXAFS.
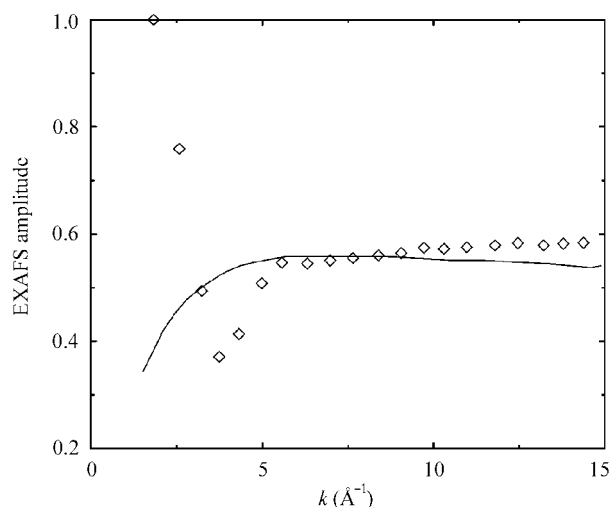
Figure 3
EXAFS loss factors for copper. The points are obtained by ratioing the EXAFS peak heights calculated using the Hedin–Lundqvist potential, which empirically includes all the losses, and the $X\alpha$ potential, which includes none. The solid line is the loss factor calculated using the screened core hole model.

Figure 4
k^3-weighted EXAFS spectra for copper foil. The solid curve shows the spectra obtained using the real $X\alpha$ potential in *EXCURV*98 multiplied by the loss factors calculated using a screened core hole. The dashed curve shows the result calculated with the Daresbury program *EXCURV*98 using the Hedin–Lundqvist exchange potential. The dotted line shows the experimental data for comparison.

In Fig. 4 we compare calculated EXAFS spectra for copper metal. To obtain the solid curve we multiply the $X\alpha$ EXAFS spectra with the calculated energy-dependent loss factor and by a mean-free-path term, with the values of the parameters as given above. The dashed line is the best-fit curve to the experimental data (dotted line) fitted using *EXCURV*98 with the Hedin–Lundqvist potential and including only a single shell of scattering atoms. The two methods of calculation appear to agree fairly well, although the agreement with experiment is poor because we have fitted using only a single shell of scattering atoms to provide an unambiguous description of the mean-free-path term. The loss factor calculated using a screened core hole is certainly more accurate than the constant s_o^2 and V_{PI} loss factors used historically.

4. Conclusion

In this paper we have used time-dependent perturbation theory and a model core-hole–photoelectron potential, $V(r)$, to obtain results for the secondary electron shake-off probabilities as a function of photon energy above the X-ray absorption edge.

We found the results to agree reasonably well with experiment. The energy dependence of the shake-off probabilities is, however, not quite correct. The dielectric function used appears to underestimate the screening at high photoelectron energies, leading to secondary electron excitation probabilities which are too large in this energy region.

The magnitudes obtained are, however, generally within the experimental error over the region of energy of interest in EXAFS. Using this method to generate an energy-dependent loss factor for EXAFS calculations would appear to give results almost as good as those obtained with the Hedin–Lundqvist potential; the advantage being that data-analysis programs using only real scattering potentials are relatively simple to write and maintain compared with those which use complex scattering potentials, especially when multiple scattering must be taken into account. The Dirac–Hara exchange potential is known to give better phase shifts for EXAFS purposes than the real part of the Hedin–Lundqvist potential (Chou *et al.*, 1987). Using this real scattering potential and an energy-dependent loss factor such as that described here we would expect to obtain good EXAFS spectra without the complications of the complex phase-shift approach.

The calculation using a screened core hole is not as accurate as the results obtained with the time-dependent model discussed in the previous paper (Roy *et al.*, 2001). The current method, however, has the advantage that it does not include 'fiddle factors'. It may point the way to a more accurate but still physically intuitive description of the loss factors, possibly using a more accurate form of the dielectric function.

References

Armen, G. B., Aberg, T., Karim, Kh. R., Levin, J. C., Crasemann, B., Brown, G. S., Chen, M. H. & Ice, G. E. (1985). *Phys. Rev. Lett.* **54**, 182–185.
Bartlett, R. J., Walsh, P. J., He, Z. X., Chung, Y., Lee, E. M. & Samson, J. A. R. (1992). *Phys. Rev. A*, **46**, 5574–5579.
Binsted, N. (1998). *EXCURV98: Computer Program for EXAFS Data Analysis.* CLRC Daresbury Laboratory, Daresbury, Warrington WA4 4AD, UK. (http://srs.dl.ac.uk/xrs/Computing/Programs/excurv97/e61.htm.)
Carlson, T. A., Nestor, C. W., Tucker, T. C. & Malick, F. B. (1968). *Phys. Rev.* **169**, 27–36.
Carter, S. L. & Kelly, H. P. (1977). *Phys. Rev. A*, **16**, 1525–1534.
Chang, T. N. & Poe, R. T. (1975). *Phys. Rev. A*, **12**, 1432–1439.

Chou, S. H., Rehr, J. J., Stern, E. A. & Davidson, E. R. (1987). *Phys. Rev. B*, **35**, 2604–2614.

Clementi, E. & Roetti, C. (1974). *Atom. Data Nucl. Data Tables*, **14**, 177–478.

Fujikawa, T., Hatada, K. & Hedin, L. (2000). *Phys. Rev. B*, **62**, 5387–5398.

Gadzuk, J. W. & Sunjic, M. (1975). *Phys. Rev. B*, **12**, 524–530.

Gradsteyn, I. S. & Ryzhik, I. M. (1965). *Tables of Integrals, Series and Products*. New York/London: Academic Press.

Gurman, S. J. (1983). *J. Phys. C*, **16**, 2987–3000.

Hasnain, S. S. (1990). Editor. *Synchrotron Radiation and Biophysics*. Chichester: Ellis Horwood.

Hayes, T. M. & Boyce, J. B. (1982) *Solid State Phys.* **37**, 173–351.

Hedin, L. (1989). *Physica B*, **158**, 344–346.

Hedin, L. & Lundqvist, S. (1969). *Solid State Phys.* **23**, 2–181.

Holland, D. M. P., Codling, K., West, J. B. & Marr, G. V. (1979). *J. Phys. B*, **12**, 2465–2484.

Natoli, C. R. (1995). *Physica B*, **209**, 5–10.

Newville, M., Livins, P. & Yacoby, Y. (1993). *Phys. Rev. B*, **43**, 14126–14131.

Noguera, C. & Spanjaard, D. (1981). *J. Phys. F*, **11**, 1133–1149.

Press, W. H., Flannery, B. P., Teukolsky, S. A. & Vetterling, W. T. (1992). *Numerical Recipes, The Art of Scientific Computing*. Cambridge University Press.

Rehr, J. J., Stern, E. A., Martin, R. L. & Davidson, E. A. (1978). *Phys. Rev. B*, **17**, 560–565.

Roy, M. & Gurman, S. J. (1997). *J. Phys. IV*, C**2** 151–152.

Roy, M. & Gurman, S. J. (2001). *J. Synchrotron Rad.* **8**, 1095–1102.

Roy, M., Lindsay, J. D., Louch, S. & Gurman, S. J. (2001). *J. Synchrotron Rad.* **8**, 1103–1108.

Samson, J. A. R., Bartlett, R. J. & He, Z. X. (1992). *Phys. Rev. A*, **46**, 7277–7280.

Thomas, T. D. (1984). *Phys. Rev. Lett.* **52**, 417–420.

Tyson, T. A. (1991). PhD thesis, Stanford University, USA.

Tyson, T. A., Hodgson, K. O., Natoli, C. R. & Benfatto, M. (1992). *Phys. Rev. B*, **42**, 5997–6019.

Vatai, E. (1988). *Phys. Rev. A*, **38**, 3777–3780.

Wight, G. R. & Van der Viel, M. J. (1976). *J. Phys. B*, **9**, 1319–1327.